atmosphere

MDPI

Article

A Study of a Miniature TDLAS System Onboard Two Unmanned Aircraft to Independently Quantify Methane Emissions from Oil and Gas Production Assets and Other Industrial Emitters

Abigail Corbett * and Brendan Smith

SeekOps, Inc., Austin, TX 78753, USA; bsmith@seekops.com
* Correspondence: acorbett@seekops.com or abbie@corbett.cc

Abstract: In recent years, industries such as oil and gas production, waste management, and renewable natural gas/biogas have made a concerted effort to limit and offset anthropogenic sources of methane emissions. However, the state of emissions, what is emitting and at what rate, is highly variable and depends strongly on the micro-scale emissions that have large impacts on the macro-scale aggregates. Bottom-up emissions estimates are better verified using additional independent facility-level measurements, which has led to industry-wide efforts such as the Oil and Gas Methane Partnership (OGMP) push for more accurate measurements. Robust measurement techniques are needed to accurately quantify and mitigate these greenhouse gas emissions. Deployed on both fixed-wing and multi-rotor unmanned aerial vehicles (UAVs), a miniature tunable diode laser absorption spectroscopy (TDLAS) sensor has accurately quantified methane emissions from oil and gas assets all over the world since 2017. To compare bottom-up and top-down measurements, it is essential that both values are accompanied with a defensible estimate of measurement uncertainty. In this study, uncertainty has been determined through controlled release experiments as well as statistically using real field data. Two independent deployment methods for quantifying methane emissions utilizing the in situ TDLAS sensor are introduced: fixed-wing and multi-rotor. The fixed-wing, long-endurance UAV method accurately measured emissions with an absolute percentage difference between emitted and mass flux measurement of less than 16% and an average error of 6%, confirming its suitability for offshore applications. For the quadcopter rotary drone surveys, two flight patterns were performed: perimeter polygons and downwind flux planes. Flying perimeter polygons resulted in an absolute error less than 36% difference and average error of 16.2%, and downwind flux planes less than 32% absolute difference and average difference of 24.8% when flying downwind flux planes. This work demonstrates the applicability of ultra-sensitive miniature spectrometers for industrial methane emission quantification at facility level with many potential applications.

Keywords: methane; oil and gas emissions; drone; UAV; mass spectrometer; COP26; biogas; biomethane; landfill; greenhouse gas

Citation: Corbett, A.; Smith, B. A Study of a Miniature TDLAS System Onboard Two Unmanned Aircraft to Independently Quantify Methane Emissions from Oil and Gas Production Assets and Other Industrial Emitters. *Atmosphere* **2022**, *13*, 804. https://doi.org/10.3390/atmos13050804

Academic Editor: James Lee

Received: 15 April 2022
Accepted: 12 May 2022
Published: 14 May 2022

1. Introduction

For decades atmospheric methane concentrations have been rising and recent public and governmental concern has spurred increased focus on accurate and reliable methane emissions improvement through monitoring, especially in the oil and gas sectors [1,2]. Currently, bottom-up estimates, such as the US Greenhouse Gas Inventory, provided by the EPA are used to estimate annual methane emissions by multiplying emission factors for each known source category by an activity factor for that source category but have limitations of accuracy and consistency [3]. Top-down estimates, where methane concentrations are used to infer emission rates, generally performed at a regional scale, sometimes leave a coarse resolution, making pinpointing leaks and single large emitters difficult [4]. To

gain a greater understanding of current North Sea emissions, the Environmental and Emissions Monitoring System (EEMS) maintained by OPRED (Offshore Regulator for Environment and Decommissioning) (https://www.gov.uk/guidance/oil-and-gas-eems-database, accessed on 14 April 2022) dataset was compiled. The majority of the emissions data reported in the EEMS dataset occurred below 13 kg/h but the data was log normal, with a max emission rate greater than 300 kg/h, as shown by the histogram of the real-world emission data in Figure 1.

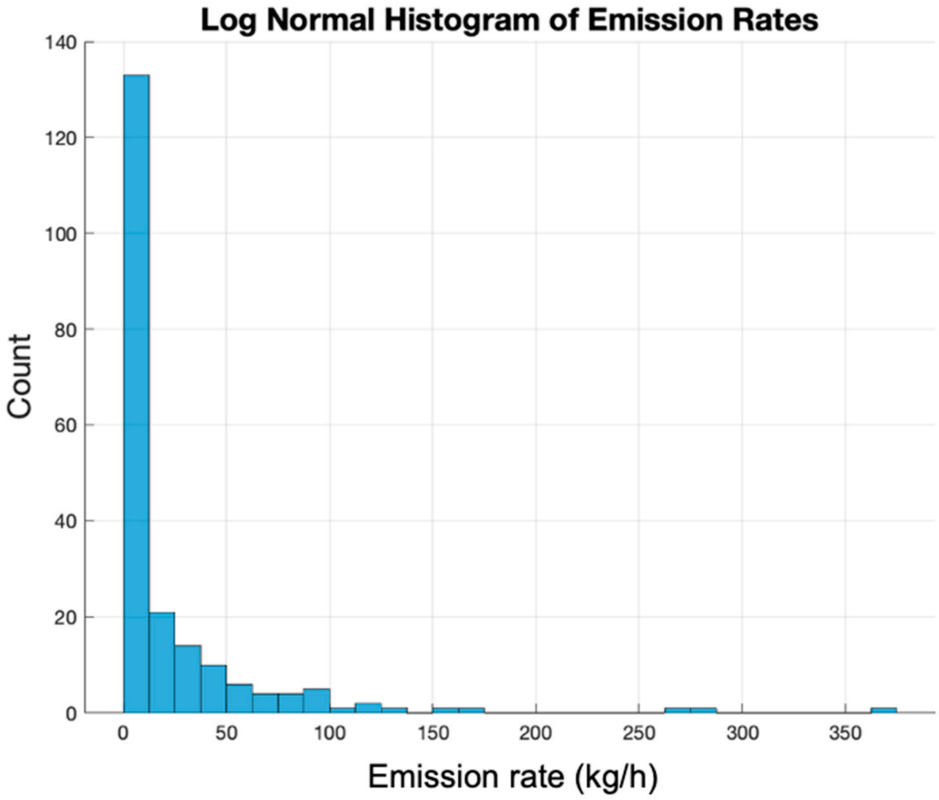

Figure 1. Histogram of EEMS top-down emissions data from North Sea offshore facilities.

Previous work in this methane emission measuring arena includes aircraft, ground and UAV platforms where lidar sensors were used to measure column-averaged methane and trace regional plumes [5]. Additionally, satellites are making their way into the methane emission measuring space as technology advances and private space companies lower historic barriers. One such example is the GHGSat-D, manufactured by GHGSat in Quebec, Canada, has quantified time average methane emissions from individual coal mine vents [6]. Other UAV based methane emission work has included mapping of emissions without supplementary ground-based measurements of a sludge deposit at a wastewater treatment plant [7].

Using a miniature methane spectrometer and long-endurance unmanned aerial vehicle (UAV), individual offshore oil and gas assets' emissions can be measured [8]. To accurately measure methane emissions in real time from assets in a large offshore oil and gas producing region, such as the North Sea, we worked with operators through the Net Zero Technology Centre (NZTC) worked together to use SeekOps small, lightweight sensor with unmanned long-distance UAV to quantify facility level emissions. The pairing of an accurate methane spectrometer sensor with an UAV allowed deployment from land to nine offshore platforms in the North Sea in 2020 and 2021, where operation interruptions were minimal and safety protocols were strictly adhered. Innovative flight patterns and novel algorithms developed to calculate mass flux from point concentration data around each asset in this study allowed for rapid processing time and demonstrated the use of this system to derive accurate

facility-level emission rates to verify current industry performance and data and highlight discrepancies from traditional bottoms-up methods [8].

The UAV-deployed quantitative gas detection solution described here has been field-proven, validated, and used to investigate methane emissions from a variety of sources including flare stacks, upstream and midstream fugitive emissions, and biogas/biomethane and landfill sites [9]. The sensor is a laser-based miniature Mid-Wave Infrared (MWIR) spectrometer capable of detecting parts per billion level changes in methane concentrations at a sampling rate of 10 Hz. These measurements coupled with change-detection algorithms enables the identification of even very small emissions. Deployment via UAV allows the sensor to more efficiently survey areas that would otherwise be difficult or unsafe to complete using handheld or stationary sensors, saving time and money. Emissions sources are surveyed by flying downwind curtains, as guided by a ground anemometer, or perimeter polygon curtains around the entire area. When desired, the area can be broken in smaller pieces, or equipment groups, as is often necessary in landfill applications, which typically cover a larger acreage than a well pad or biogas facility. Once the methane measurements have been recorded, the data is uploaded and processed to give an emission rate estimation.

To better understand methane emissions from offshore platforms, we performed a remote methane survey of facilities in the North Sea. These flights served as the first comprehensive methane emissions survey of an offshore platform with a miniature methane spectrometer onboard a UAV [10]. This new approach provided fit for purpose "top-down" emissions measurements required to meet the goals of emission data verification. The purpose of the project leading up to the 2020 campaign was to develop a method for detecting and quantifying methane emissions from any offshore facility globally. The approach measured site-level total methane emissions from either outside or within the operational exclusion zone of offshore facilities. Similar to onshore reporting, current offshore methane emissions reporting requires "bottom-up" accounting, which in well-metered instances are reported with a high degree of confidence but for unmetered sources can lead to significant uncertainty in the calculated emissions. With the advent of compact, low weight, sensitive sensors, high resolution aerial measurements, and innovative algorithms for emission rate calculation, this new technology is now available for accurate emissions quantification. The integration of these developments enabled quantification of emissions rates that can verify calculated bottom-up values and give the facility operator an improved understanding of their methane performance. Beyond the reporting implication of this approach, this method(s) may lead to early identification of emissions issues from a safe distance that are unobtrusive to normal operations.

2. Materials and Methods

The in situ methane sensor used in this work is a laser-based miniature MWIR spectrometer capable of detecting parts per billion level changes in methane concentrations. More detail on sensor performance can we read in Smith et al. [8]. The sensor is designed to be either mounted in the bottom of a fixed-wing unmanned aerial vehicle (UAV) or mounted on the front end of a quadcopter drone, so readings are not influenced by the propellor wash out, as shown in Figure 2. Use of a fixed-wing drone enables much longer duration flights than its rotorcraft counterpart and has allowed for unobtrusive long-range surveys of offshore assets to be conducted, whereas the use of rotorcraft allow greater resolution between equipment groups—allowing precise locations of emissions to be resolved. The choice of aircraft can therefore be made to reflect the type of emission data being obtained. The performance of the closed-cell methane sensor was characterized by multiple in-lab, ground, and flight tests.

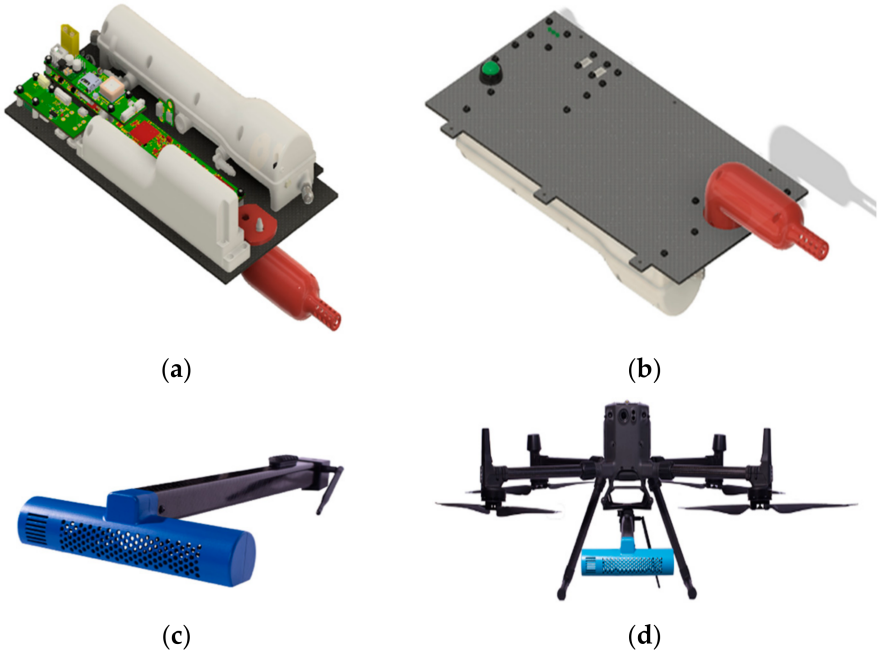

Figure 2. Sensor payloads (**a**) showing the top of the fixed-wing version, (**b**) showing the bottom of the fixed wing version, (**c**) showing the completely independent sensor housing and arm for rotary drones, (**d**) showing the sensor mounted on the front of a quadrotor drone.

A key aspect of the specific solution described here is a process for emissions rate quantification that is based on a standard engineering control volume model. There are three major contributions to this process: (1) the fast response in situ gas sensor, (2) an optimal flight pattern design, (3) proprietary analysis methods that allow for rapid and accurate quantification.

To survey methane from assets and platforms offshore, beyond visual line of sight (BVLOS) flights originating from shore (e.g., airfield, airstrip, airport) were conducted using a long-range UAV and the miniature laser spectrometer integrated below the flight surface. The preferred flight pattern designed to accurately survey methane emissions while accounting for flight limitations, such as flight time and range, was selected through a combination of plume modelling and flight path simulations [8]. These simulations yielded an optimal flight envelope radius of 250 m and an altitude profile of 0–185 m. However, the optimal flight pattern was not always feasible due to the safety restrictions of assets. A normal exclusion zone is 500 m, but the UAV can be granted permission to fly closer when low emission rates are expected based on bottom-up averages. However, when a facility has floating components, a larger standoff distance may be used to allow for vessel movement around a central axis. Through closed surface flight paths such as these, flowrates can be calculated.

During our helix flight pattern, the fixed-wing aircraft flew at a constant radius around the asset's furthest point from the center. A simplified schematic of the fixed-wing flight pattern is shown in Figure 3. The aircraft started the testing event at the set radius from the asset being surveyed at the highest sampling altitude. Once at the set radius, the aircraft spiraled down in a counterclockwise pattern from the maximum altitude, ~210 m (700 ft) above ground level (AGL) stepping down at a consistent vertical step to the lowest altitude, usually around 30.48 m (100 ft) AGL at a constant speed of 30 m per second. Once at the lowest safe altitude, the aircraft will spiral up at the same altitude step in the counterclockwise direction flying between the previous laps, creating an interlaced track. Flying between the spiral down altitudes on the upward section of the flight path increases the vertical resolution of the data while limiting the time dependency of altitude and emission. This spiral down then immediate spiral up flight pattern will be referred to

as "down–up" or DU for the duration of this document. With a standard standoff distance of 300 m and a drone speed of ~31 m/s, surveys usually take around 30 min to complete.

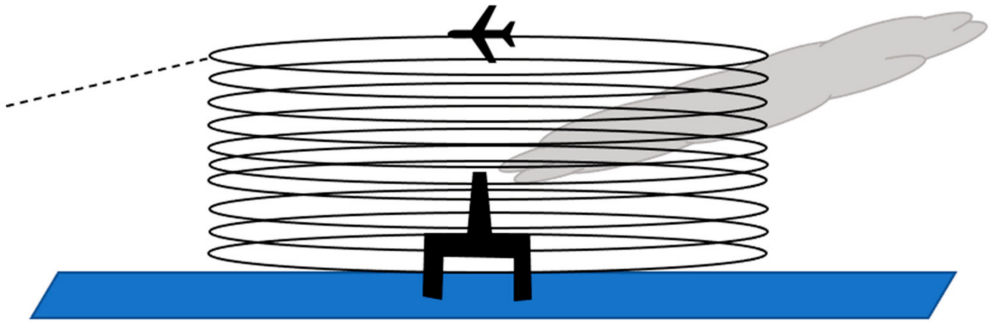

Figure 3. Schematic showing the Helix flight pattern used on the fixed-wing drone where the path is shown in black circles around a simplified asset, and the emissions being surveyed is shown as a gray cloud. The black dashed line is the point where the UAV enters the survey area around the asset. The standard standoff distance used in the controlled release experiment is 250 m from the furthest most point. A 300 m radius flight pattern was used in the controlled release experiment.

For the quadrotor drone, two flight patterns have been developed. The first involved the pilot flying the drone a safe distance downwind of a potential emission source, as determined by the safety guidelines and an anemometer. This flight pattern has been proven successful in controlled release and field campaigns [11]. Once a plume is located using the streamed methane concentrations displayed on the ground control system, a curtain pattern was flown starting at the lowest altitude up to the highest to completely envelope any emissions as seen on the ground control unit and an immediate decent in the same area interlacing the ascent path. For a full survey, this pattern was flown twice. Figure 4 shows a schematic of this flight path. These flight patterns are useful as they take a short amount of time to complete. They also require minimal flight planning and air traffic permissions due to the relatively short altitude range. Lastly, due to the impromptu nature, smaller areas can be isolated and surveyed individually, allowing for equipment group level estimations of emission rates. These flux plane or curtain-like flight paths usually take about 30 min to complete, depending on the horizontal length of the flight path. If the horizontal distance is large in the case of landfills, surveys can take a few hours to complete.

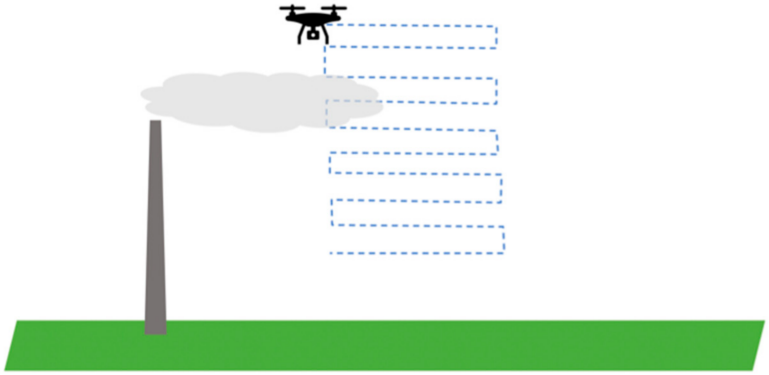

Figure 4. Schematic showing the rotary drone ascent during flux plane flight pattern where the flight path is shown in the dashed line and the emissions is shown as a gray cloud.

Another flight pattern deployed using the quadrotor drone has been termed the perimeter method, where polygons around the emission point were flown at altitude intervals creating a closed surface similar to the helix flight pattern used for the fixed-wing.

The drone traced the polygons at ascending altitude heights and then descended, interlacing the altitudes flown during the ascent. Figure 5 shows a schematic of the perimeter flight path. These flight paths guarantee quantifications from the survey are from within the perimeter sampled, limiting outside influence of neighboring emitters. Additionally, these flight patterns were automated and so are useful when comparisons over time are desired as they ensure the comparison is like to like. These types of flight patterns take longer to complete than the flux plane or curtains due to the linear distance needed to complete.

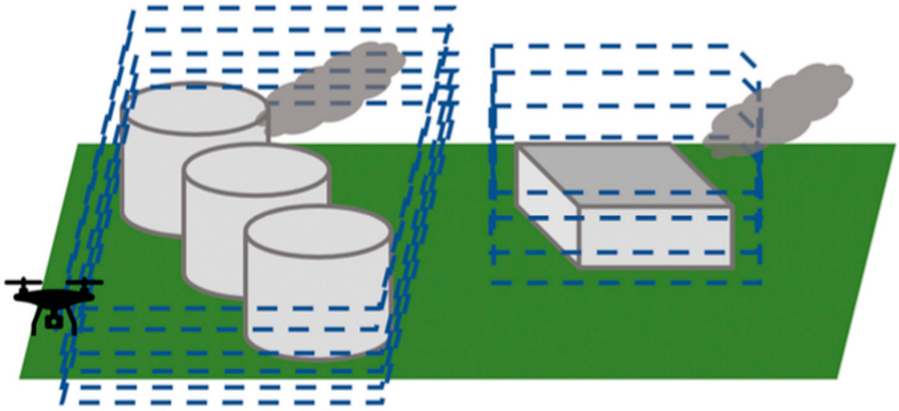

Figure 5. Schematic showing the rotary drone perimeter flight pattern where the flight path is shown in dashed blue and the simplified emission sources is shown in grey.

As mentioned previously in Table 1, the sensor measures instantaneous methane mole fractions at a 10 Hz sampling rate. The helical mass flux emission quantification analysis method ingests volumetric mixing ratios and calculates the mass flux encapsulated in either the perimeter or the helix flight pattern resulting in a kilogram per hour emission rate of the encapsulated area, using a Lagrangian mass balance and Gaussian Theorem approach adapted from Nathan et al.'s paper that used a model aircraft to survey a compressor station [12].

Table 1. SeekIR Methane Sensor information, two configurations.

Sensor	
Weight	850 g
Sensitivity	10 ppb/s
Format	Time-series concentrations
Flow Rate (L/min)	9.0 L/min
Temperature range	5 °C to 45 °C
Battery life	10 h

The mass balance approach was chosen over a classic Gaussian plume equation due to the dependence of Gaussian plume approaches on a large number of variables including stack height, stability class from the Pasquill–Gifford scale, wind profile exponent, stack temperature, stack tip diameter and stack velocity, requiring additional information and lot of involvement of operators of the sources of emissions [13]. Operators may not record such variables at frequent intervals or be reluctant to provide such information; thus, Gaussian plume estimations would limit surveying potential and greatly increase the dependency of emitter involvement in the calculation of emissions.

For the helix and perimeter flight patterns, data from the sensor methane sensor and the aircraft log files are recorded through the entire flight and then the individual laps are isolated around the emitter using algorithms that separate the laps around the emission

source giving each lap a relatively uniform altitude and more individualized representation of the wind. The emission rate is calculated using Equation (1):

$$E = \int \oint w_l \sin\alpha \, \rho_{air}(x_{lz} - x_z) dl dz \quad (1)$$

where the integrand is the path integral for each lap, or horizontal advective flux, where w_l is the mean horizontal wind speed during that lap derived from the UAV log files in the case of the fixed-wing, α is the angle relative to the mean wind at that sampled point in the lap such that at the most downwind moment, the alpha term, $\sin\alpha$, equals one and as the measurements are taken around the counterclockwise lap the alpha term slowly decreases until at the points directly upwind the alpha term equals -1. ρ_{air} is the density of air calculated using the ideal gas law with pressure and temperature of the air in the sensor measured at that point in the lap, and x_{lz} is the methane mole fraction measured at that point in the lap. Without the account for real-world sampling effects, the summation of the alpha term around each lap equals 0; however, due to those real-world influences of sampling each methane measurement is not precisely equidistant and thus influences the lap integral. To account for this, the integral with constant methane concentration for the entire lap is subtracted from the integral of the methane measurements. Though this is a closed-loop integral, we use a smoothing x_z term to minimize any influence of sampling density (i.e., slight changes in speed of the UAV, instantaneous wind measurements, loop stepping) that would make the integral with a constant methane mole fraction not equal to 0. Due to the preprogrammed flight pattern and advanced flight tracking system, each lap is assumed to have equal vertical thickness. This assumption has been validated and any derivation from the equal height is minimal. Figure 6 shows an example of a lap identified in the helix pattern where (a) shows the flight path colored for methane concentration in parts per billion, (b) shows the flight path colored by the alpha term, showing the area with the largest influence on the lap integral in the flight path is where the flight path is normal to the wind direction, (c) shows a time series in UTC seconds where the alpha term in plotted and the horizontal advective flux (HAF) in grams per meters squared seconds. As expected, the highest HAF occurs where the largest intersection of an emission is noted by the yellow color showing increased methane and the locational alpha term is also at the highest, denoting its most downwind location in the lap.

For the flux plane rotary drone flight pattern, data from the sensor methane sensor are recorded through the entire flight and then the individual curtains are isolated. A ground-based anemometer was set up on-site to measure wind speed and direction. Once the data is collected for a curtain, the data is interpolated onto a grid and projection to the normal of the mean wind direction as illustrated in Figure 7.

Because we only measured the wind at anemometer height of 1.5 m, we used a standard log law vertical wind gradient equation to estimate the wind speeds at altitudes where the survey occurred not represented by the anemometer. The emission rate is calculated using Equation (2):

$$E = \iint w_z \rho_{air} \left(x_{yz} - x_{background} \right) dy dz \quad (2)$$

where w is the altitude binned wind speed using a ground-based anemometer and log wind profile estimation, ρ_{air} is the air density calculated using measured temperature and pressure, x_{yz} average concentration measured in that grid cell, and $x_{background}$ is the concentration measured in an upwind section of the survey.

Controlled release experiments were designed to gain a better understanding of the empirical uncertainty of the methods, and a more detailed appreciation of the assumptions that go into the analysis. The sensor had been validated and calibrated in a laboratory setting, but to understand the validity of these methods at quantifying methane emissions, we needed to compare the sensor deployment, processing algorithms, and techniques to a metered source. These controlled release experiments aided in the understanding of how

well the flight patterns sample the plume, and how accurately the method calculates the emission rate at varied emission rates and flight radiuses.

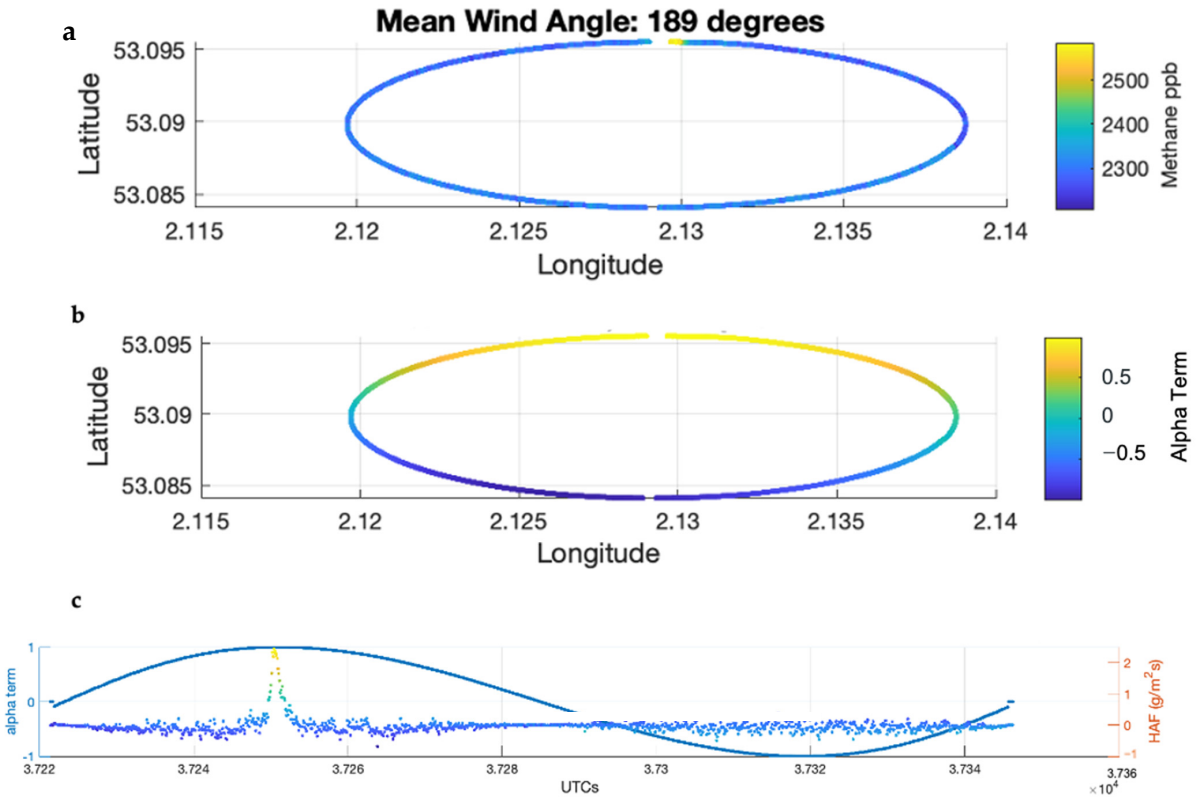

Figure 6. (**a**) Lap flight path colored by methane; (**b**) lap flight path colored for alpha term. Note the alpha term is largest downwind, and smallest most upwind; (**c**) timeseries of lap overlapping the alpha term and the HAF.

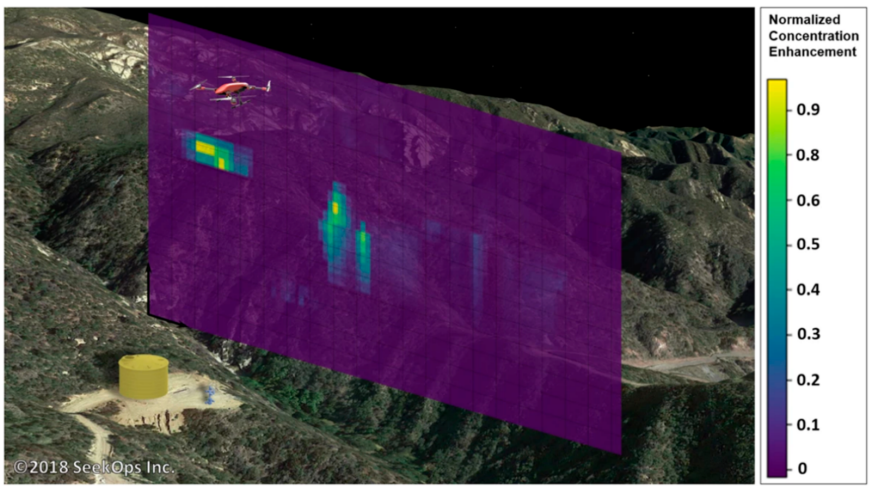

Figure 7. A 3-Dimensional illustration of the flux plane flight pattern measurement process. Elevated methane concentrations are interpolated onto a continuous grid, multiplied by the corresponding wind vector and spatially integrated to quantify the source emission rates.

The test objectives were as follows:

- Determine the efficacy of emission detection for variable rates at different distances from the emission source;

- Ensure the repeatability of flux calculation as the distance from the emission source is increased;
- Ensure that the majority of the plume is accurately transected during flight patterns;
- Verify the independence of emission rate estimate accuracy to the actual emission rate;
- Define the empirical uncertainty of the methods by calculating the relative error of the actual release rate against the calculated rate.

The following variables in Table 2 were either logged or controlled during the flights. A certified gas meter was used to verify emission rates throughout the tests and the methane supplied was lab certified and traceable with datasheets.

Table 2. List of variables in controlled release experiment.

Logged	Controlled
Time of day	Flight Pattern
Methane concentrations (ppb)	Methane release rates (0–25 kg/h) as monitored by a certified gas meter
Temperature (K)	
Pressure (mbar)	
Windspeed (m/s)	
Wind direction (degrees)	

The controlled release experiment took place at Deenethorpe Airfield located 2 miles east of Corby, Northamptonshire, England where we were able to control aircraft in the region and adhere to strict airfield safety protocols. We used a mass flow controller with digital readings to control the flow of the methane at set points throughout the experiment.

To most mimic real-world emissions, a 56 m tall crane was used to elevate the release point, as shown in Figure 8.

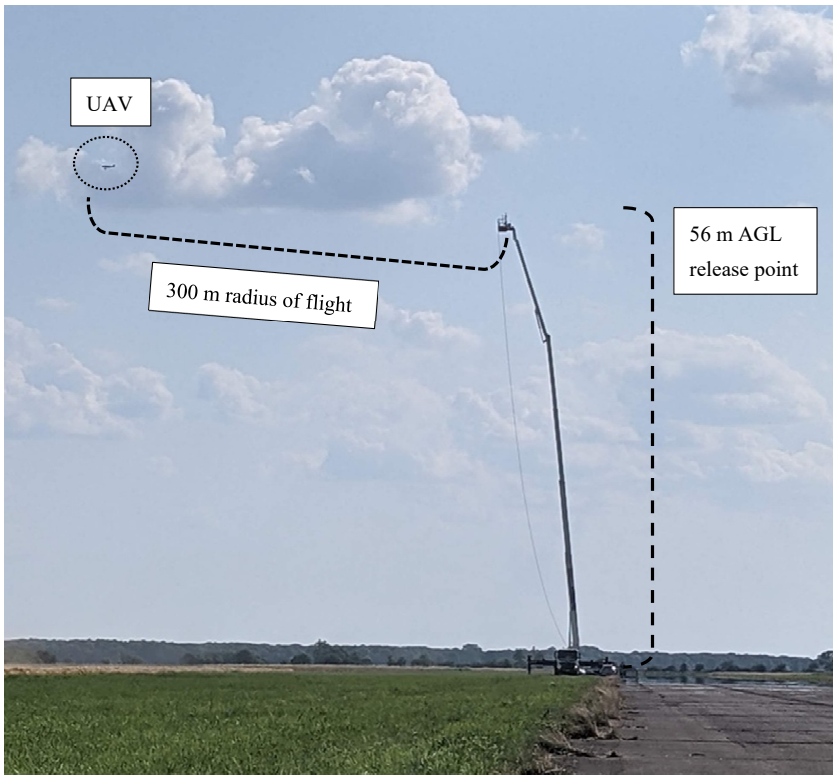

Figure 8. 56 m tall crane holding the emission point, connected by braided tubbing to flow meter sitting on the runway as the fixed-wing UAV flies a 300 m radius helical flight pattern on 22 July 2021 at Deenthorpe Airfield, UK.

Table 3 outlines the fixed-wing UAV controlled release experiment, specifically identifying the emission flow rates, releasing CH_4 at 55 m (180 ft) height above the ground, flight pattern, step size (10 m or 25 m), and the date each testing event occurred. Test event order was chosen to limit any correlation between parameters outside of the experiment control, such as weather and wind, with measured sensor data.

Table 3. Summary of fixed-wing controlled release tests flown in a helix pattern at 300 m radius from the emission source that was elevated on a 56 m tall crane.

Flow Rate (kg/h)	Vertical Step Distance (Meters)	Date Completed
3	10	22 July 2021
3	25	21 July 2021
3	25	21 July 2021
6	10	21 July 2021
6	10	21 July 2021
6	25	22 July 2021
6	25	22 July 2021
9	10	20 July 2021
9	10	20 July 2021
9	25	20 July 2021
13	10	22 July 2021
13	25	20 July 2021
15	25	21 July 2021
15	25	21 July 2021
20	25	22 July 2021
20	25	22 July 2021
25	25	21 July 2021
25	10	21 July 2021
25	10	21 July 2021
6	10	22 July 2021
20	10	22 July 2021
0	25	21 July 2021
0	25	20 July 2021
0	25	22 July 2021

Table 4 outlines the quadrotor UAV controlled release experiment, specifically identifying the emission flow rates, releasing CH_4 at 55 m (180 ft) height above the ground, flight pattern, and the date each testing event occurred. The test event order was chosen to limit any correlation between parameters outside of the experiment control, such as weather and wind, with measured sensor data.

Table 4. Summary of rotary drone controlled release tests flown in either flux plane or perimeter flight patterns around the emission source that was elevated on a 56 m tall crane. For flux plane flight patterns (FP) the stand of distance is also noted in meters.

Flow Rate (kg/h)	Date Completed	Flight Pattern
0	23 July 2021	FP/300 m
0	23 July 2021	FP/50 m
0	26 July 2021	FP/50 m
0	27 July 2021	Perimeter
1	27 July 2021	FP/50 m
3	23 July 2021	FP/300 m
3	23 July 2021	FP/50 m
3	23 July 2021	FP/50 m
3	26 July 2021	Perimeter
6	23 July 2021	FP/300 m
6	26 July 2021	Perimeter

Table 4. *Cont.*

Flow Rate (kg/h)	Date Completed	Flight Pattern
9	23 July 2021	FP/300 m
9	23 July 2021	FP/50 m
9	26 July 2021	FP/50 m
9	26 July 2021	Perimeter
12	27 July 2021	Perimeter
15	23 July 2021	FP/300 m
15	26 July 2021	Perimeter
25	23 July 2021	FP/50 m
25	23 July 2021	FP/200 m
25	26 July 2021	FP/50 m
25	26 July 2021	Perimeter

3. Results

3.1. SeekIR on Fixed Wing UAV

During the fixed-wing flights, an interwoven cylindrical pattern was flown around the asset to quantify emissions. Table 5 shows all the release rates and corresponding number of tests and the one sigma confidence interval of the corresponding tests during the fixed-wing experiment.

Table 5. Summary of fixed wing drone controlled release tests flown around the emission source that was elevated on a 56 m tall crane showing release rate as shown on the flow meter, number of tests completed at that rate, and the 1 sigma confidence interval.

Release Rate	Number of Tests Completed	1σ (68%) Confidence Interval
0 kg/h	3	-0.49 ± 1.3 kg/h
3 kg/h	4	1.18 ± 1.3 kg/h
6 kg/h	4	7.12 ± 13.2 kg/h
9 kg/h	4	2.92 ± 1.7 kg/h
13 kg/h	2	1.85 ± 0.5 kg/h
15 kg/h	3	9.11 ± 3.7 kg/h
20 kg/h	4	1.15 ± 1.8 kg/h
25 kg/h	4	13.03 ± 12.1 kg/h

In order to further understand the results, we isolated the changing variables and found a strong inverse correlation between accuracy and wind speed, as shown in Figure 9. At lower winds (<3 m/s), the percent difference is significantly and consistently higher. There is a negative trend between wind speed and percentage difference, meaning as wind speed increases, the difference decreases. Atmospheric stability, or the tendency of the atmosphere to resist or enhance vertical motion and thus turbulence, is determined by wind speed and solar insolation. An unstable atmosphere enhances turbulence, whereas a stable atmosphere inhibits mechanical turbulence. Though we saw low winds and an unstable atmosphere in our experiment that took place in the summer over land, we are unlikely to experience that offshore where wind speeds are not expected to be less than 3 m/s more than a few days a year. Atmospheric stability is generally more stable over water where the water takes longer to heat and cool when compared to earth.

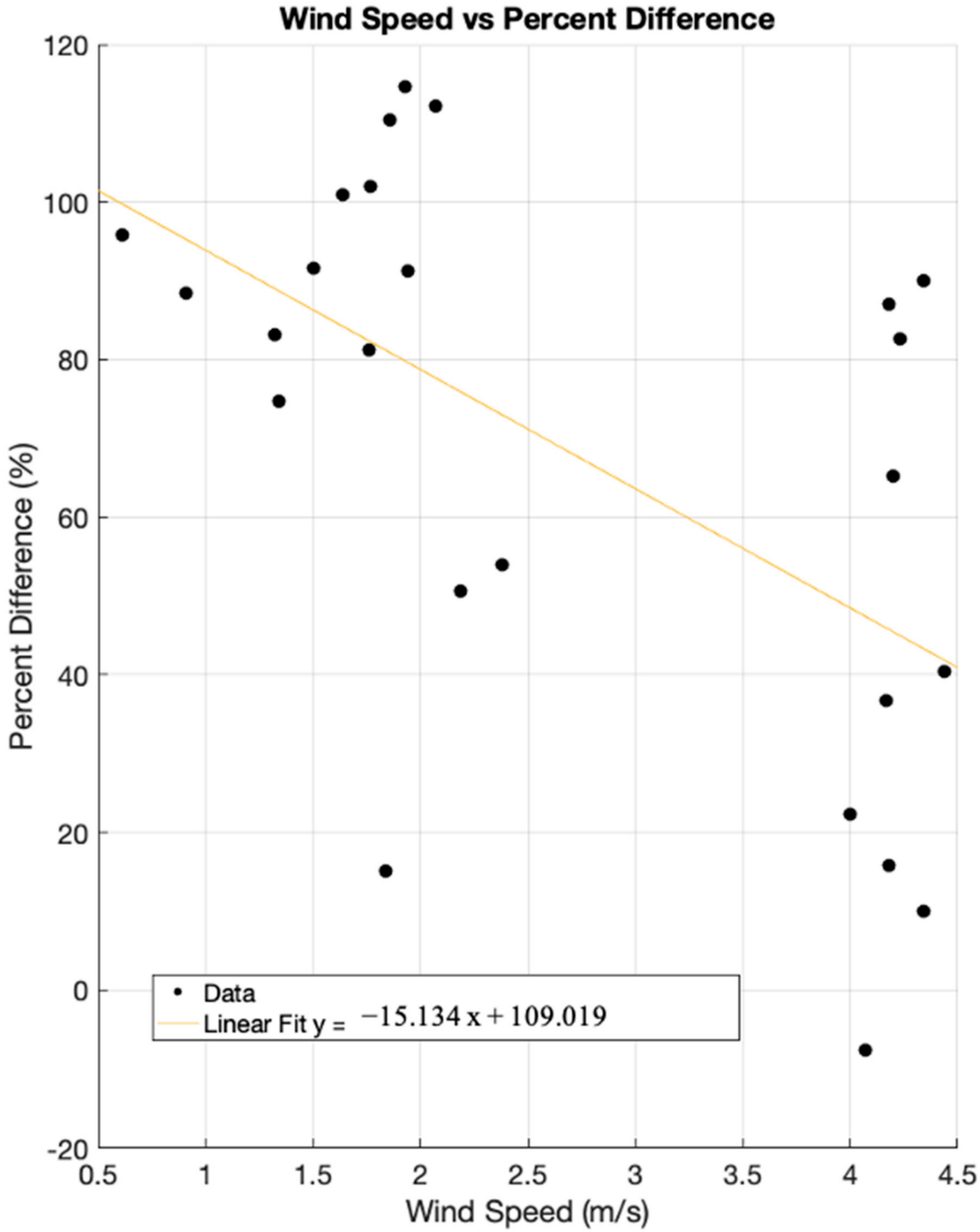

Figure 9. Scatter plot showing the wind speed versus the percentage difference. Note the negative trend line with a slope of −1.5.

When we limit the experiment to surveys that occurred in stable atmospheric conditions where wind was greater than 3 m/s and emission plumes are known to behave in a predictable conical pattern, the number of tests dropped from 28 to 10. Table 6 shows the 10 tests and the corresponding release rate and confidence intervals. However, one important item to note is the data density also varied in our experiment by varied flight patterns and altitude step heights.

Table 6. Summary of fixed-wing drone controlled release tests flown around the emission source that was elevated on a 56 m tall crane when the atmospheric stability was stable, and the wind was greater than 3 m/s.

Release Rate	Number of Tests	1σ (68%) Confidence Interval
3 kg/h	3	1.67 ± 1.1 kg/h
15 kg/h	3	9.1 ± 3.7 kg/h
25 kg/h	4	13.03 ± 12.1 kg/h

When we further limited our surveys, to wind greater than 3 m/s and the preferred data density as shown in the flight pattern and altitude step, only 3 tests remained as shown in Table 7. The percent difference greatly decreases, and we see accuracy that would be seen in offshore applications where wind speeds are greater than 3 m/s more than 360 days a year.

Table 7. Summary of fixed-wing drone controlled release tests flown around the emission source that was elevated on a 56 m tall crane when the atmospheric stability was stable, the wind was greater than 3 m/s., and the flight path allowed a larger data density.

Release Rate	Number of Tests	Result	Absolute Difference
3 kg/h	1	2.7 kg/h	10%
15 kg/h	1	12.6 kg/h	16%
25 kg/h	1	26.9 kg/h	8%

The mean absolute difference we expect to see in offshore environments is 11.3%. We expect differences less than 16% in offshore applications, such as the North Sea. Future work includes conducting a similar controlled release test in an actual offshore setting, with a metered emission source. This would most realistically show the atmospheric conditions of an offshore environment and how they affected our empirical uncertainty.

3.2. SeekIR on Rotary Drones

3.2.1. Flux Plane Flight Pattern

As described previously, during the downwind flux plane, a vertical raster pattern is flown using a quadrotor UAV normal to the mean wind direction in the downwind direction. The horizontal length of the flux plane is usually determined based on available area at the asset site and is controlled live by a pilot who is monitoring methane readings using a livestream handheld unit. The drone starts at the lowest safe altitude and flies the horizontal section and then the drone steps up 2 m vertically and completes the following horizontal section at the new altitude before descending and interlacing the previous altitudes. Table 8 shows the flux plane tests completed during the controlled release with their corresponding standoff distance, wind speed, the mean observed flow rate during the test as displayed by the flow rate meter, the calculated rate, and the absolute percent error. Note that error calculations are not possible for the control rates of 0 kg/h; however, these tests are important to note because the calculated rate is also 0 kg/h, meaning there was not a false detection of emissions. The absolute error ranges from 1.19 to 88.36%. The average absolute percent error for all the tests is 28.1%.

Figure 10 shows a scatter plot showing the detected rate in kg/h versus the metered flow rate observed in kg/h. The 1:1 line is shown in black for reference and the linear fit is shown as a dashed line with an R^2 value of 0.8236.

Table 8. Rotary drone controlled release tests flown in flux plane flight patterns around the emission source that was elevated on a 56 m tall crane.

Flow Rate (kg/h)	Standoff Distance (m)	Mean Wind (m/s)	Mean Observed Flow Rate (kg/h)	Calculated Rate (kg/h)	Absolute Error (%)
0	300	4.0	0.00	0.00	-
0	50	5.8	0.00	0.00	-
0	50	1.7	0.00	0.00	-
1	50	3.1	1.00	1.20	20.00
3	300	4.8	2.93	3.12	6.67
3	50	5.7	2.92	5.50	88.36
3	50	4.5	2.73	2.70	1.19
6	300	5.1	5.98	4.00	33.11
9	300	5.3	9.12	8.00	12.30
9	50	4.3	9.00	11.70	30.00
9	50	1.8	9.48	6.20	34.63
15	300	5.4	15.95	18.00	12.85
25	50	4.7	24.97	36.00	44.17
25	200	4.1	25.64	20.00	22.01
25	50	5.5	25.74	17.50	32.02

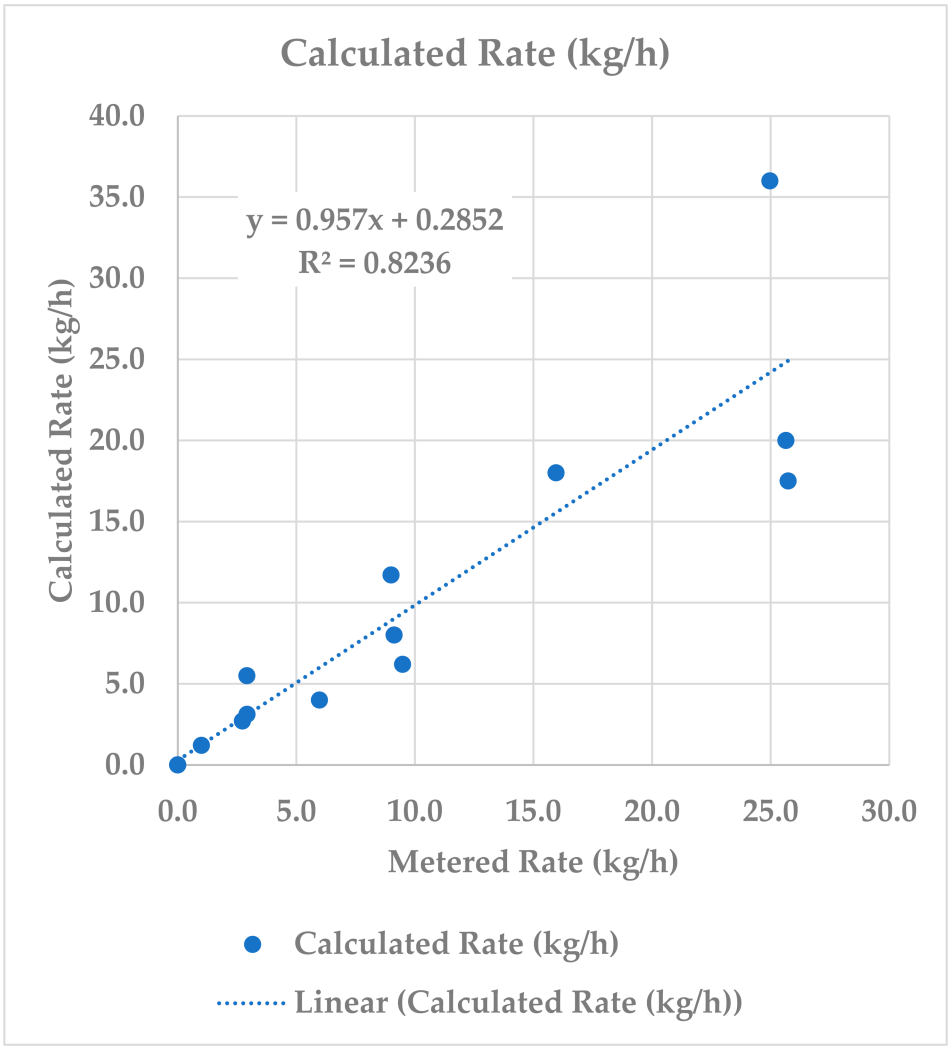

Figure 10. Scatter plot showing the metered rate in kg/h versus detected emission calculated in kg/h in blue. The linear fit is shown in a dashed blue line.

The emission rate quantification is calculated using the wind vector. Wind speed affects plume behavior and is measured during the quadrotor drone sensor deployment using an anemometer. Figure 11 shows a scatter plot of absolute error versus wind speed showing a negative correlation between absolute error and wind speed. This follows what one would expect for a mass balance equation, where low wind speeds can have negative impacts on the accuracy.

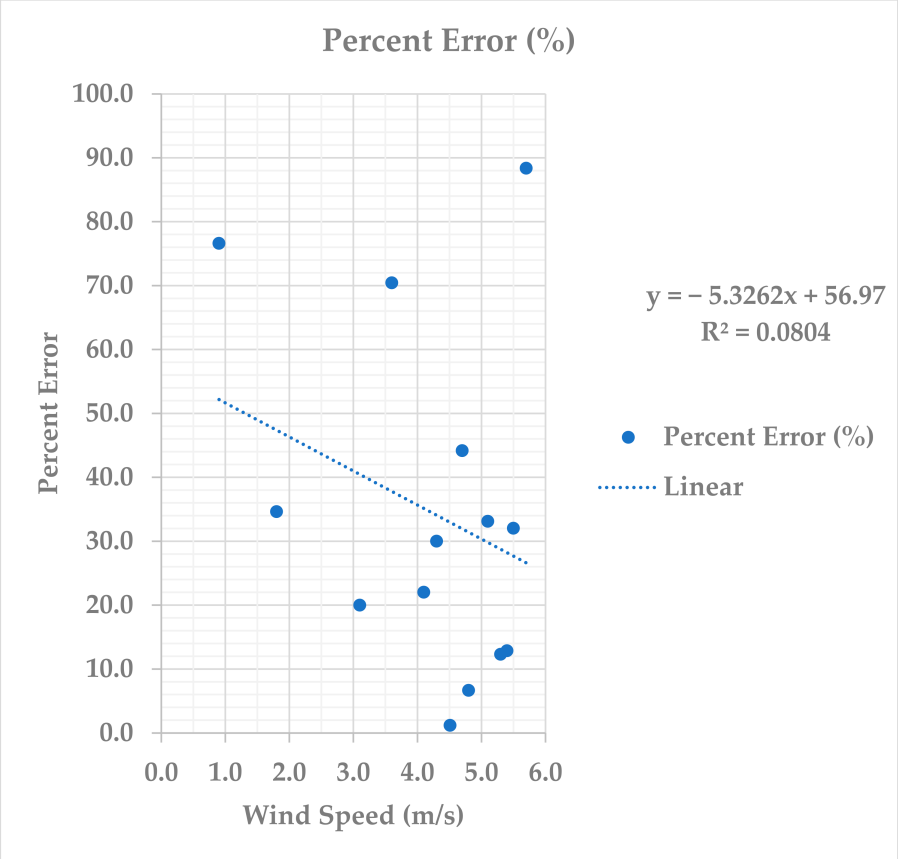

Figure 11. Scatterplot of absolute error of flux plane flight pattern tests versus wind speed. A negative correlation is shown in the linear fit line in yellow and the linear fit equation of y = −5.32x + 56.97.

Where repeat tests occurred, we grouped the tests into similar flow rates and calculated the mean absolute error of each flow rate, the mean absolute error ranged from 13–32%, as shown in Table 9. There does not seem to be a correlation between flow rate and error. For flow rates with more than 1 test completed, the 1 sigma confidence interval was calculated by calculating the variance of the group.

Table 9. Rotary drone controlled release tests flown in flux plane flight patterns around the emission source grouped by flow rate. The number of tests completed at that flow rate is shown, as well as the 1 sigma confidence interval when more than 1 test was performed. The mean absolute error is calculated by averaging the absolute errors of tests at that flow rate.

Flow Rate (kg/h)	Number of Tests	1σ (68%) Confidence Interval	Mean Absolute Error
1	1	1.2 kg/h	20%
3	3	3.7 ± 1.5 kg/h	32%
6	1	4	33%
9	3	8.6 ± 2.8 kg/h	26%
15	1	18	13%
25	3	25 ± 10 kg/h	25%

3.2.2. Perimeter Flight Patterns

During the perimeter rotary drone controlled release, perimeter polygons were flown as described in previous sections. The drone flies stacked polygons around the release point at stepped altitude intervals, mimicking flights flown along access roads and paths around assets. Benefits include the automated nature that does not change based on wind direction, the limited potential influx from sources upwind of the release point, and the reproducibility of future surveys for accurate temporal evolution statistics. Table 10 shows the release rates, the mean observed flow rate displayed on the flow meter, the calculated rate and the absolute error when comparing the calculated to the observed flow rate.

Table 10. Summary of rotary drone controlled release tests flown in perimeter flight pattern around the emission source that was elevated on a 56 m tall crane.

Flow Rate (kg/h)	Mean Observed Flow Rate (kg/h)	Calculated Rate (kg/h)	Absolute Error (%)
0	0	0.0	-
3	3.10	3.31	6.6
6	6.29	8.54	35.7
9	9.38	10.12	7.9
12	12.50	14.57	16.6
15	15.51	13.30	14.3

Figure 12 shows a scatter plot of observed flow rate vs. calculated emissions rate for the perimeter rotary drone tests with an R^2 value of 0.9219.

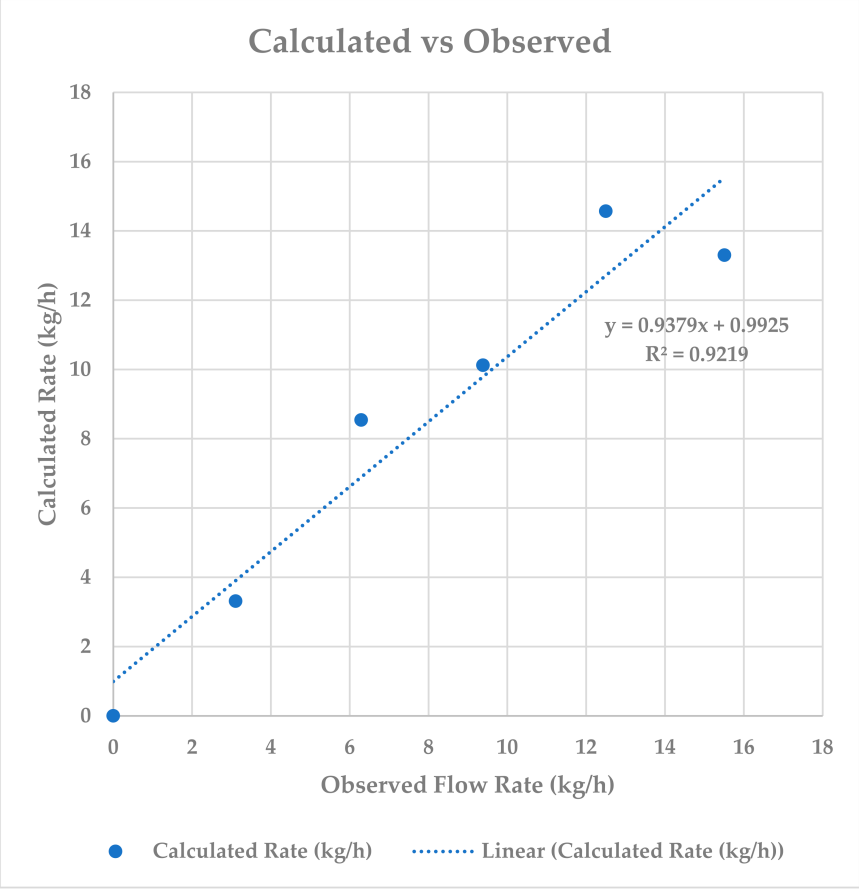

Figure 12. Scatterplot of absolute error of perimeter flight pattern tests release rates versus calculated emission rates. The R^2 equal to 0.9219.

4. Discussion

Atmospheric stability, or the tendency of the atmosphere to resist or enhance vertical motion and thus turbulence, is determined by wind speed, direction, and solar insolation where a potential temperature profile is not available. An unstable atmosphere enhances turbulence, whereas a stable atmosphere inhibits mechanical turbulence. For the lowest uncertainty, it is optimal to survey during neutral or stable conditions as proven by the increased uncertainty of the 18 fixed-wing tests in unstable conditions. Though we observed low winds and an unstable atmosphere in our experiment, we are unlikely to experience that in offshore environments. Atmospheric stability is generally more stable over water, where the water takes longer to heat and cool when compared to earth.

This experiment confirms the fixed-wing DU helix pattern at 300 m standoff distance intercepts the plume. The data shows that the sensor can perform accurately when compared to a metered emission source. The method calculated emission rates accurately (within $\pm$16%) at higher atmospheric stability across the range of emission rates released (3–25 kg/h) when using the fixed-wing to deploy the sensor. This shows promising accuracies for offshore applications and applications when site access or very close proximity is not possible. The uncertainties in this experiment described the sensor, flightpath, and method(s) during mostly unstable atmospheric conditions, which are unlikely in usual surveying conditions for fixed-wing applications (primarily offshore). This experiment gave greater insight into how flight patterns and atmospheric conditions can affect our results, and we will use this knowledge in the planning of future surveys to ensure that uncertainties are minimized.

The flux plane flight pattern using the rotary drone, at both the 50 m and 300 m standoff distances, surveys the plume. The flux plane flight pattern, coupled with the previously described concentration to rate inversion method, accurately surveys emissions within 33% when full flights are performed and winds are greater than 1 m/s. The rotary drone is an accurate, reliable, flexible, and time-efficient alternative to a fixed-wing drone with a successful history onshore and has potential applications offshore, particularly when direct platform access is not practical.

5. Conclusions

Internal, regulatory, and societal pressures to limit methane emissions has in turn spurred innovation and technology development for measurement and mitigation of methane emissions. Simultaneously, large strides in unmanned aerial vehicle technology has enabled precision measurement in extreme environments (e.g., offshore oil and gas facilities). The oil and gas industry has a history of leading such innovations in measurement and participating in industry-wide efforts such as the Oil and Gas Methane Partnership (OGMP). OGMP pushes for accurate global accounting of emissions using best available technology and respecting the nuances of global operations, all while enabling a standardized approach that is not prescriptive. It is up to the industry to suggest appropriate methods and best practices that can meet the critical goals set forth by OGMP 2.0.

The lightweight, rugged in situ sensor in presented in this study proves that methane measurements can be collected in an operationally efficient and consistent manner that is appropriate for methane measurement and reduction goals of the industry. Furthermore, it is shown that leveraging small UAV technology is critical to methane emission reduction goals and can be used to not only detect methane emissions, but also robustly quantify them. Using empirically collected controlled release data, this work has highlighted that deterministic analysis of methane concentration measurements from a sensitive mobile spectrometer combined with wind data can yield accurate and robust asset-level emission rates from offshore oil and gas operations, and other methane emitting industries such as landfills and biogas.

Robust autonomous data processing procedures have been established allowing for a one-to-one comparison of repeat surveys, while guaranteeing that surveys fall within the accuracy and uncertainties described. This standardization of data acquisition and

processing allows repeat surveys to be compared and compiled for greater understanding of asset emissions, as well as over time add to the statistics of similar sites and regions. The automated processing techniques used in this study allow for a short processing time, enabling near real-time actionable information and, therefore, facilitating faster remedial action. Faster remedial action and mitigation saves customers money all while limiting further emissions, benefitting the climate.

The standardized flight patterns used in this study adequately measure the methane emissions, take approximately 30 min to complete, and therefore offer minimal disruptions to assets normal operating procedure. With limited disruption, these surveys can be utilized at temporal intervals to gain accurate insights into not only facility-level emissions but also equipment group-level emissions in the case of the quad rotor applications. The sensor, standardized quantification methods, and automated algorithm suites perform accurately and consistently when compared to a metered emission source. This gives us great confidence in the method in quantifying emissions in the real-world applications, especially oil and gas production surveys that our experiment was designed to mimic. Additionally, this experiment gave greater insight on how flight patterns, intrinsically data density, and atmospheric conditions can affect emission quantification results. We use this knowledge in the survey planning to ensure the best results with the smallest uncertainties.

As industries continue to strive toward net-zero, new technologies such as those described in this work will continue to be developed an fill any gaps in industry knowledge. Accurate measurement of emissions is the first step to mitigating and reducing emissions. Using these methods, industries will be able to gain accurate emissions quantifications and reduce their emissions for the betterment of the global climate, all while deploying in a manner that is cognizant and meets the broader stakeholder interests.

Author Contributions: Conceptualization, A.C. and B.S.; methodology, A.C.; software, A.C.; validation, A.C.; formal analysis, A.C.; investigation, A.C.; resources, B.S.; data curation, A.C.; writing—original draft preparation, A.C.; writing—review and editing, A.C. and B.S.; visualization, A.C.; supervision, B.S.; project administration, A.C.; funding acquisition, B.S. All authors have read and agreed to the published version of the manuscript.

Funding: This research was funded by Net Zero Technology Centre, with partnership of bp, Equinor, Harbor Energy, Shell, Taqa, and Total.

Institutional Review Board Statement: Not applicable.

Informed Consent Statement: Not applicable.

Data Availability Statement: Not applicable.

Acknowledgments: Flylogix, NZTC, Operators, especially bp for their contribution to the rotary drone controlled release experiment. Special thanks to Zeeco for their work supplying and metering methane during the controlled release.

Conflicts of Interest: The authors are employees of SeekOps Inc., the designer and manufacturer of the miniature TDLAS sensor presented in this study.

References

1. Etheridg, D.M.; Steele, L.P.; Francey, R.J.; Langenfelds, R.L. Atmospheric methane between 1000 A.D. and present: Evidence of anthropogenic emissions and climatic variability. *J. Geophys. Res. Atmos.* **1998**, *103*, 15979–15993. [CrossRef]
2. Konschnik, K.; Jordaan, S.M. Reducing fugitive methane emissions from the North American oil and gas sector: A proposed science-policy framework. *Clim. Policy* **2018**, *18*, 1–19. [CrossRef]
3. *Inventory of U.S. Greenhouse Gas Emissions and Sinks: 1990–2019*; Environmental Protection Agency: Washington, DC, USA, 2021.
4. Vaughn, T.L.; Bell, C.S.; Pickering, C.K.; Schwietzke, S.; Health, G.A.; Petron, G.; Nummedal, D. Temporal variability largely explains top-down/bottom-up difference in methane emission estimates from a natural gas production region. *Proc. Natl. Acad. Sci. USA* **2018**, *115*, 11712–11717. [CrossRef] [PubMed]
5. Refaat, T.F.; Ismail, S.; Nehrir, A.R.; Hair, J.W.; Crawford, J.H.; Leifer, I.; Shuman, T. Performance evaluation of a 1.6-μm methane DIAL system from ground, aircraft and UAV platforms. *Optics Express* **2013**, *21*, 30415–30432. [CrossRef] [PubMed]
6. Varon, D.J.; Jacob, D.J.; Jervis, D.; McKeever, J. Quantifying Time-Averaged Methane Emissions from Individual Coal Mine Vents with GHGSat-D Satellite Observations. *Environ. Sci. Technol.* **2020**, *54*, 10246–10253. [CrossRef] [PubMed]

7. Gålfalk, M.; Påledal, S.N.; Bastviken, D. Sensitive Drone Mapping of Methane Emissions without the Need for Supplementary Ground-Based Measurements. *Earth Space Chem.* **2021**, *5*, 2668–2676. [CrossRef] [PubMed]
8. Smith, B.; Buckingham, S.; Touzel, D.; Corbett, A.; Tavner, C. Development of Methods for Top-Down Methane Emission Measurements of Oil and Gas Facilities in an Offshore Environment Using a Miniature Methane Spectrometer and Long-Endurance UAS. In Proceedings of the SPE Annual Technical Conference and Exhibition, Dubai, United Arab Emirates, 21–23 September 2021.
9. Ravikumar, A.P.; Sreedhara, S.; Wang, J.; Englander, J.; Roda-Stuart, D.; Bell, C.; Brandt, A.R. Single-blind inter-comparison of methane detection technologies—Results from the Stanford/EDF Mobile Monitoring Challenge. *Elem. Sci. Anthr.* **2019**, *7*, 37. [CrossRef]
10. Tavner, C.A.; Touzel, D.F.; Smith, B.J. Application of Long Endurance UAS for Top-Down Methane Emission Measurements of Oil and Gas Facilities in an Offshore Environment. In Proceedings of the SPE Offshore Europe Conference & Exhibition, Virtual, 7–10 September 2021.
11. Allen, D.; Stokes, S.; Tullos, E.; Smith, B.; Herndon, S.; Flowers, B. Field Trial of Methane Emission Quantification Technologies. In Proceedings of the SPE Annual Technical Conference and Exhibition (ATCE 2020), Denver, CO, USA, 5–7 October 2020; OnePetro: Richardson, TX, USA, 2020.
12. Nathan, B.J.; Golston, L.M.; O'Brien, A.S.; Ross, K.; Harrison, W.A.; Tao, L.; Zondlo, M.A. Near-Field Characterization of Methane Emission Variability from a Compressor Station Using a Model Aircraft. *Environ. Sci. Technol.* **2015**, *49*, 7896–7903. [CrossRef] [PubMed]
13. Pasquill, F. The estimation of dispersion of windborne material. *Met. Mag.* **1961**, *90*, 33–49.